Petroleum Science 20 (2023) 2796–2808

Contents lists available at ScienceDirect

Petroleum Science

journal homepage: www.keaipublishing.com/en/journals/petroleum-science

Original Paper

Response analyses on the drill-string channel for logging while drilling telemetry

Ao-Song Zhao [a, b], Xiao He [a, b, c, *], Hao Chen [a, b, c], Xiu-Ming Wang [a, b, c]

[a] State Key Laboratory of Acoustics, Institute of Acoustics, Chinese Academy of Sciences, Beijing, 100190, China
[b] University of Chinese Academy of Sciences, Beijing, 100049, China
[c] Beijing Engineering Research Center of Sea Deep Drilling and Exploration, Institute of Acoustics, Chinese Academy of Sciences, Beijing, 100190, China

ARTICLE INFO

Article history:
Received 22 August 2022
Received in revised form
2 February 2023
Accepted 13 March 2023
Available online 15 March 2023

Edited by Jie Hao

Keywords:
Logging while drilling
Borehole geophysics
Downhole acoustic telemetry
Channel modeling
Frequency selectivity

ABSTRACT

Downhole acoustic telemetry (DAT), using a long drill string with periodical structures as the channel, is a prospective technology for improving the transmission rate of logging while drilling (LWD) data. Previous studies only focused on the acoustic property of a free drill string and neglected the coupling between pipes and fluid-filled boreholes. In addition to the drill-string waves, a series of fluid waves are recorded in the DAT channel, which has not been investigated yet. Unpredictable channel characteristics result in lower transmission rates and stability than expected. Therefore, a more realistic channel model is needed considering the fluid-filled borehole. In this paper, we propose a hybrid modeling method to investigate the response characteristics of the DAT channel. By combining the axial wavenumbers and excitation functions of mode waves in radially layered LWD structures, the channel model is approximated to the 1-D propagation, which considers transmission, reflection, and interconversion of the drill-string and fluid waves. The proposed 1-D approximation has been well validated by comparing the 2-D finite-difference modeling. It is revealed that the transmitted and converted fluid waves interfere with the drill-string wave, which characterizes the DAT channel as a particular coherent multi-path channel. When a fluid-filled borehole surrounds the drill string, the channel responses exhibit considerable delay as well as strong frequency selectivity in amplitude and phase. These new findings suggest that the complexity of the channel response has been underestimated in the past, and therefore channel measurements on the ground are unreliable. To address these channel characteristics, we apply a non-coherent demodulation strategy. The transmission rate for synthetic data reaches 15 bps in a 94.5 m long channel, indicating that the acoustic telemetry is promising to break the low-speed limitation of mud-pulse telemetry.

1. Introduction

Effective communication between downhole and surface instruments has become a critical need in logging while drilling (LWD), as real-time acquisition and interpretation of downhole data streams enable engineers to mitigate drilling risks and optimize wellbore trajectories. Conventional mud-pulse telemetry has data rates normally below 3 bits per second, which hardly meet the increasing demand for LWD data transmission (Klotz et al., 2008; Wassermann and Kaniappan, 2009). Besides, this technology is unsuitable for underbalanced drilling scenarios because of the highly compressible drilling fluid (Gao et al., 2006). Given the limitations of mud-pulse telemetry in applications, downhole acoustic telemetry (DAT) using the drill-string channel can be a prospective alternative (Tochikawa et al., 1996; Shah et al., 2004; Neff and Camwell, 2007; Reeves et al., 2011). However, strong scattering occurs when the drill-string wave passes through periodically arranged tool joints, resulting in the alternate distribution of passbands and stopbands, also known as the bandgap characteristic. Since the 1990s, many researchers have investigated the acoustic property of the free drill string. Drumheller (1989) first approximated the drill string as a 1-D periodic waveguide and developed a finite-difference time-domain algorithm to simulate the propagation of drill-string waves. This approximation strategy

* Corresponding author. State Key Laboratory of Acoustics, Institute of Acoustics, Chinese Academy of Sciences, Beijing, 100190, China.
E-mail address: hex@mail.ioa.ac.cn (X. He).

https://doi.org/10.1016/j.petsci.2023.03.007

has been validated to be reasonable in the frequency band for communication (Lee, 1991; Rama Rao and Vandiver, 1999). Then, using the fourth-order Runge-Kutta technique, Carcione and Poletto (2000) expanded the theory and developed a time-domain algorithm for the propagation of low-order axial, torsional, and flexural waves. In addition to numerical methods in the time domain, analytical techniques in the frequency domain were also proposed. By applying continuity conditions of displacement and stress at the interface, the drill-string assembly was modeled as a two-port network of propagation matrix to obtain reflection and transmission coefficients (Lous et al., 1998; Wang et al., 2006; Gutierrez-Estevez et al., 2013; Kumar et al., 2014). Some ground tests showed that these modeling methods could accurately predict the bandgap distribution when the drill string is measured in air (Gutierrez-Estevez et al., 2013; Zheng et al., 2017).

However, in LWD operations, due to the presence of drilling liquid and the formation, the transmission environment of the DAT channel can be more complex. Rama Rao and Vandiver (1999) pointed out that two fluid-related modes would be simultaneously excited in the DAT channel in addition to the drill-string wave. These two modes are commonly referred to as the outer Stoneley wave and the inner Stoneley wave, called fluid waves in this paper. Field data showed that fluid waves would increase the channel delay and interfere with the drill-string wave, leading to strong frequency selectivity in the passband (Drumheller, 1993; Drumheller and Knudsen, 1995). Unpredictable channel characteristics result in lower transmission rates and stability than expected. Although some previous studies (Rama Rao and Vandiver, 1999) theoretically investigated the propagation mechanism of drill-string and fluid waves, they modeled the steel pipe as two-layer uniform cylindrical surfaces without considering the periodically cascaded tool joints. These tool joints act as scattering sources and can directly lead to coupled propagation of guided waves, which in turn makes the DAT channel response very complex. In the actual situation, attention should be paid to the contributions of both transmitted and scattered waves. Therefore, a more realistic model is needed to investigate the response characteristics of the DAT channel.

In recent years, studies on the monopole LWD wavefield and the design of LWD isolators have attracted our attention. Mode waves excited in a radially layered borehole will interact with the surrounding media and exhibit various wave behaviors. It is revealed that the dispersion, attenuation, and excitation of LWD mode waves are all affected by the surrounding medium parameters (Cui, 2004; Sinha et al., 2009; Zheng and Hu, 2017; He et al., 2017). These waveguide properties can be attributed to the axial wavenumber and excitation function of the mode wave, which needs to be considered in the DAT channel modeling. As for LWD isolators, Matuszyk and Torres-Verdín (2014) and Yang et al. (2017) found that grooves on the surface of a drill collar prolonged the duration of the collar wave and converted part of the collar-wave energy into long-duration fluid wavetrains. The fluid waves converted from collar waves have considerable amplitudes. Note that the structure of the LWD isolator is also axially periodic, just like a short drill string. Thus the wavefield variations caused by grooving can be instructive for our issue. In fact, from the field tests of the DAT channel, it is found that the delay spread of the channel is several times larger than the estimated value, even if only the drill-string-wave arrival was intercepted (Drumheller, 1993; Drumheller and Knudsen, 1995). Combined with the observations of Matuszyk and Torres-Verdín (2014) and Yang et al. (2017), it is reasonable to speculate that part of drill-string waves has been converted into fluid waves at the tool joint, leading to a considerable channel delay. However, the converted fluid waves cannot be simulated by the existing channel modeling, which are parts of the carrier waves and strongly coupled with the transmitted drill-string waves. Lacking systematic theoretical studies, the adverse impacts of significant mode conversion on channel performance are still unknown. Incomplete knowledge of the DAT channel will inevitably lead to the failure of ground demodulation, thus limiting the transmission rate and reliability.

In this article, we first review the dispersion and attenuation properties of DAT modes. Then, the calculations of the near-source excitation function help determine the appropriate source and receiver deployment. By combining the axial wavenumber and excitation function of mode waves, we propose a novel 1-D model for the DAT channel. Four continuity conditions are used to construct the propagation matrix network. The transmitted and converted waves can therefore be simulated and discussed separately. And the channel function of the DAT channel is formulated. The accuracy of the proposed method is well validated by comparing the synthetic full waveforms with the 2-D finite-difference. Then we analyze the impulse response, amplitude-frequency response, and group delay of the DAT channel, respectively, while taking the drill-string channel in a vacuum as a reference. Finally, we observe the carrier modulation in the DAT channel and propose a robust data transmission strategy. According to the synthetic data, it is practicable to combine carrier multiplexing and non-coherent demodulation to achieve efficient data transmission using the DAT channel.

2. Theory of channel modeling

The channel modeling of the downhole acoustic telemetry (DAT) is divided into two parts. First, the propagation and excitation characteristics of the DAT modes are solved and discussed, and the axial diameter variations of the drill string are not yet considered. Then, we approximate the DAT channel to a 1-D model in the z-axis direction. The channel is a periodic structure with N units.

2.1. Propagation and excitation of DAT modes

The DAT channel can be modeled as an open waveguide with a concentric cylindrically-layered structure, as shown in Fig. 1. The radial layers from inside to outside the borehole are the inner fluid cylinder, the drill string, the outer fluid annulus, and the infinite formation, respectively. The drill string consists of a periodic cascade of drill pipes and tool joints, and the ends of the drill string are assumed to be an infinite length in the z-direction. We define an (r, z) cylindrical coordinate system and let the borehole axis be the z-axis. Moreover, an annular source is mounted on the outer surface of the drill pipe, and the axial position corresponds to $z = 0$. Studies by Zheng et al. (2004) and Pardo et al. (2013) show that in the acoustic telemetry band (generally below 1 kHz), the tool eccentricity does not generate new propagating modes. And the effect on wave dispersion and excitation can be very slight when the degree of eccentricity is not significant. Therefore, we believe modeling the DAT channel as concentric hardly affects the calculation results.

In order to theoretically evaluate the DAT mode dispersion and excitation, it is necessary to treat the drill string as a uniform long pipe and ignore the periodic tool joints. In this case, the physical model becomes a multi-layered cylindrical structure with uniform surfaces, equivalent to acoustic logging while drilling (LWD). The dispersion properties of the DAT mode can be obtained by the dispersion equation which is derived as (Cui, 2004; Sinha et al., 2009)

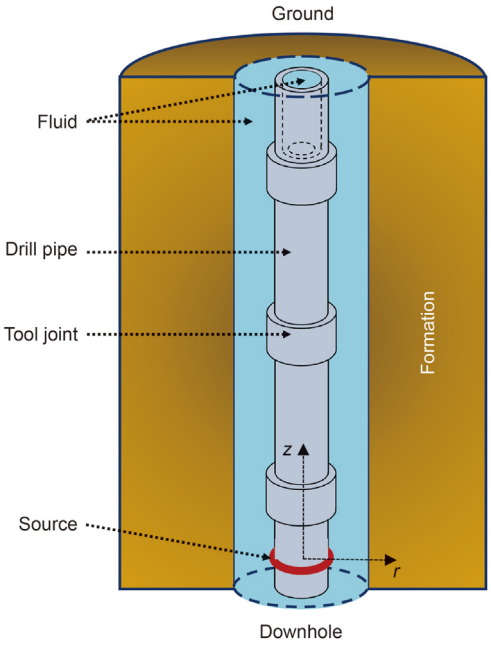

Fig. 1. The sketch of a radially layered model for the DAT channel at the (r, z) cylindrical coordinates. From inside to outside, the four layers are the inner fluid cylinder, the drill string, the outer fluid annulus, and the infinite formation, respectively. The drill string consists of a periodic cascade of drill pipes and tool joints.

$$|\mathbf{D}(k_z, \omega, r)| = 0 \tag{1}$$

where k_z is the z-axial wavenumber; ω is the angular frequency; r refers to the radial position of each interface; $\mathbf{D}$ is the matrix representing the wavefield of a multi-layered cylindrical structure, and the detailed mathematical expression for the matrix $\mathbf{D}$ has been given by Cui (2004). In particular, R_1, R_2, and R_3 are the inner and outer radii of the drill string and the borehole radius, respectively. By solving Eq. (1), the poles of the mode waves $k_z = k_{\text{pole}}(\omega)$, also called the mode wavenumber, can be obtained. Note that poles are complex-valued. The real part of the mode wavenumber gives the dispersion characteristics, while the imaginary part provides the attenuation characteristics of the modes, which are computed as

$$v_{\text{phase}}(\omega) = \frac{\omega}{\text{Re}\left[k_{\text{pole}}(\omega)\right]} \tag{2}$$

$$\alpha(\omega) = 20\log_{10} e^{\text{Im}\left[k_{\text{pole}}(\omega)\right]} \tag{3}$$

It is necessary to explain that Eq. (3) indicates the amplitude attenuation per meter when the mode wave propagates in the traveling direction (i.e., z-direction). Here the attenuation value is expressed logarithmically in decibels. The phase velocity and attenuation curves of the DAT modes can be depicted from Eqs. (2) and (3), respectively, as shown in Fig. 2. The carrier frequencies for downhole communication are generally in the weak-dispersion low-attenuation band, so the frequency range of interest is set to 0–6 kHz. To simulate the dissipation effect of the fluid-filled borehole, we introduce quality factors into fluids and the formation. Detailed parameters for simulations are listed in Table 1. The outer radius of each layer is based on the data in the "drill pipe" column. Note that the 4-in standard drill pipe is used for simulations, consistent with Drumheller (1989) and Wang et al. (2006). Fig. 2a presents the phase velocity curves, from which three propagating modes, including the drill-string wave, inner Stoneley wave, and outer Stoneley wave, can be distinguished in the DAT channel. The drill-string wave indicates the first-order drill-string mode, whose velocity is slightly lower than the P velocity of the drill string. The inner Stoneley wave is the interfacial wave propagating at the interface between the inner fluid and the drill string. Its speed is close to the fluid acoustic velocity. The outer Stoneley wave propagates at the interface between the outer fluid and the formation, and its speed mainly depends on the fluid acoustic velocity (Rama Rao and Vandiver, 1999). It is also found that the dispersion effects of these three waves are almost negligible in such a low-frequency range. Then, from Fig. 2b, the attenuations of all three modes are frequency-dependent, reflecting the coupling of mode wave propagation with the fluid-filled borehole. The unit of attenuation values has been converted to dB/km in Fig. 2b.

The relative amplitudes of the mode waves in the DAT channel are related to not only the propagation loss but also the near-source excitation function. To evaluate the excitation characteristic, we introduce an axisymmetric source in the form of boundary condition as

$$\tau_{rz(2)} = \sigma_s, \text{ at } r = R_2 \tag{4}$$

where the field quantity $\tau_{rz(2)}$ denotes the shear stress component at the outer radius of the drill string; the symbol σ_s denotes the shear-stress source applied at the outer pipe wall. Because the drill-string wave exhibits axial vibration in the frequency band of interest, the shear-stress source is more suitable for exciting the drill-string wave than the normal-stress source applied in acoustic LWD (Lee, 1991; Rama Rao and Vandiver, 1999). The mode wave arrivals are contributed by the poles in the complex wavenumber plane, so the excitation function can be evaluated by calculating the residues of the field components at the poles (Kurkjian and Chang, 1986; Kurkjian, 1985)

$$\text{Exc}(\omega) = \left.\frac{\text{i}e^{\text{i}k_z z} \cdot p(\omega, k_z, r)}{\partial|\mathbf{D}(\omega, k_z, r)|/\partial k_z}\right|_{k_z = k_{\text{pole}}(\omega)} \tag{5}$$

where i is an imaginary unit; $p = \rho_f \omega^2 \varphi_f$ is fluid pressure, where ρ_f is fluid density and φ_f is the displacement potential of the fluid layer. Since receivers are generally exposed to fluid, it is appropriate to receive the fluid pressure.

We fix the receiver-to-source axial distance at $z = 0.5$ m to obtain the near-source excitation functions. Fig. 3 compares the near-source excitation amplitudes when the receivers are placed at two radial positions. The amplitudes in the figures are the absolute value of the excitation function calculated in Eq (5). Fig. 3a shows the case where the receiver is mounted on the inner surface of the drill pipe (i.e., $r = R_1$). In this case, the excitation amplitudes of the drill-string wave are the largest among the three modes and present no decay in the whole frequency range. Fig. 3b shows the results received on the outer surface of the drill pipe (i.e., $r = R_2$). In this case, the excitation amplitudes of the drill-string wave are lower than the Stoneley waves, and the decay appears between 3 kHz and 4 kHz. Based on this comparative analysis, we determine that the receiver should be deployed on the inner surface of the drill pipe to obtain a stronger drill-string wave. The results in Fig. 3a also demonstrate that the source loading method in Eq. (5) is appropriate for our problem; that is, the drill-string wave with strong amplitude and no decay is excited. However, note that the total amplitudes of two fluid modes are roughly equivalent to those of the drill-string wave, which indicates that the interference of fluid waves on the DAT channel can not be negligible.

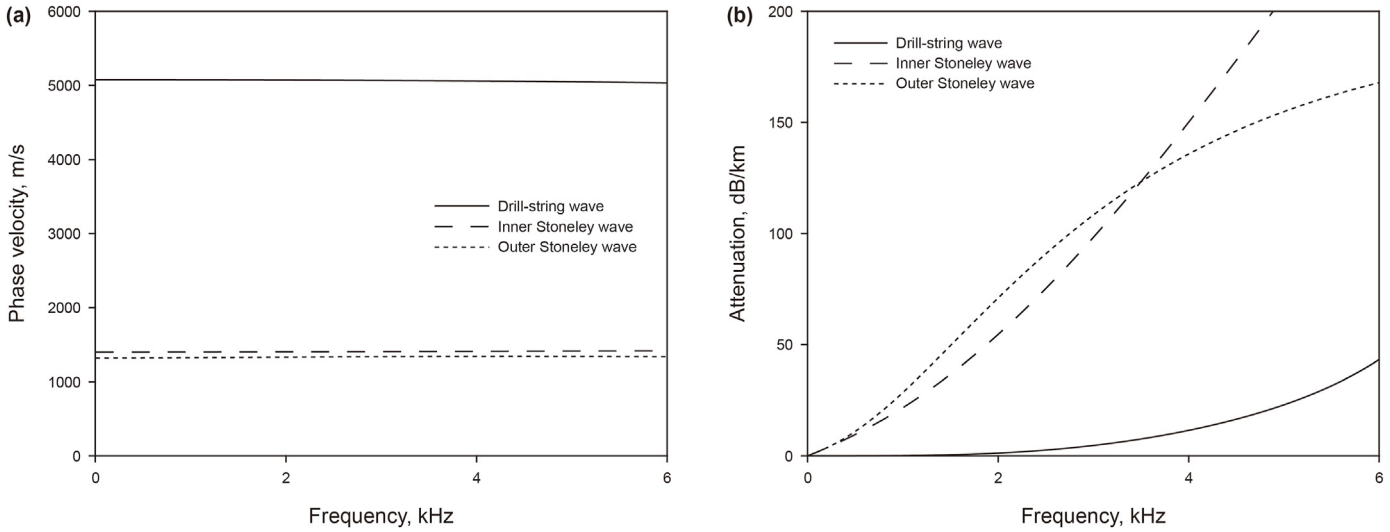

Fig. 2. (a) Phase velocity and (b) attenuation curves of DAT mode waves. In order to theoretically evaluate the DAT mode dispersion, it is necessary to treat the drill string as a uniform long pipe and ignore the periodic tool joints.

Table 1
Model parameters for the simulations.

	Density, kg/m^3	P velocity, m/s	S velocity, m/s	Outer radius, m		Quality factor
				Drill pipe	Tool joint	
Inner fluid	1000	1470	–	0.042	0.041	1000
Drill string	7800	5860	3130	0.051	0.076	–
Outer fluid	1000	1470	–	0.120	0.120	1000
Formation	2320	3972	2455	∞	∞	60

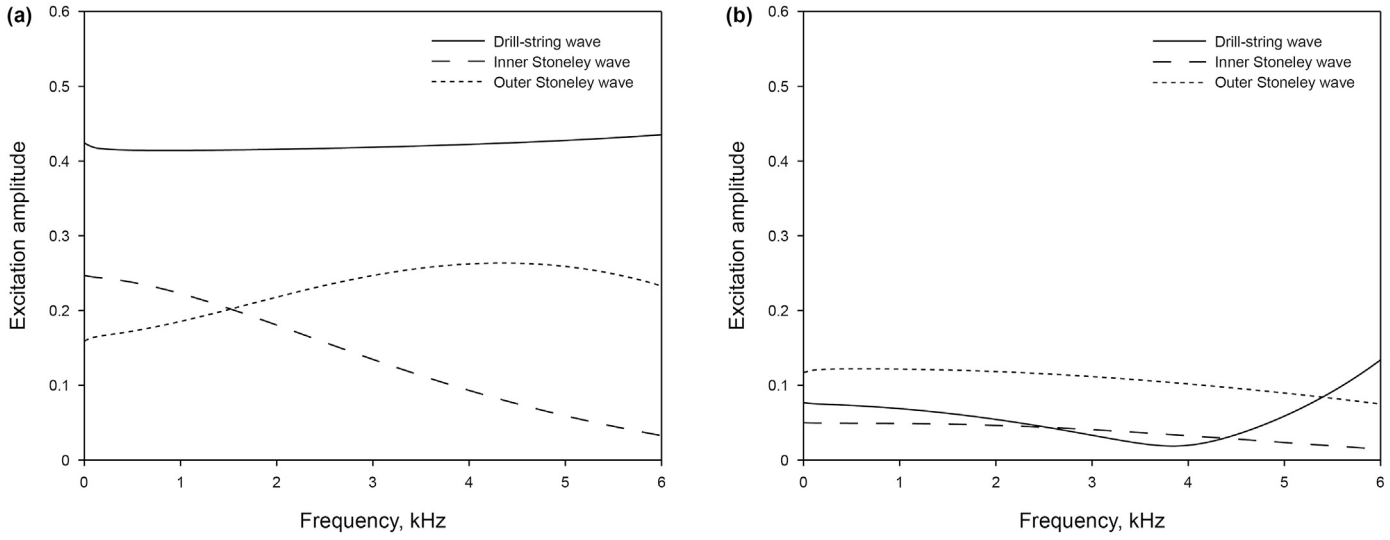

Fig. 3. The near-source excitation amplitudes of DAT modes. The source is mounted on the outer surface of the drill pipe, and the receiver-to-source axial distance is fixed at $z = 0.5$ m. The radial locations of the receiver are (a) the inner surface (i.e., $r = R_1$) and (b) the outer surface (i.e., $r = R_2$) of the drill pipe, respectively.

2.2. Calculation of channel function

By investigating displacement profiles, Lee (1991) and Rama Rao and Vandiver (1999) revealed that three DAT modes present axial vibration characteristics in the frequency range of interest, which is the basis for approximating the DAT channel to a 1-D model. To further simplify the problem, we assume that the inner Stoneley wave only interacts with the cross-section variations in the inner fluid. Similarly, the outer Stoneley wave is considered to interact only with cross-section variations in the outer fluid. This way, the transmission of these two fluid waves in the DAT channel can be calculated separately.

The 1-D modeling of the DAT channel is depicted in Fig. 4. Both fluid waves and the drill-string wave are regarded as 1-D waves

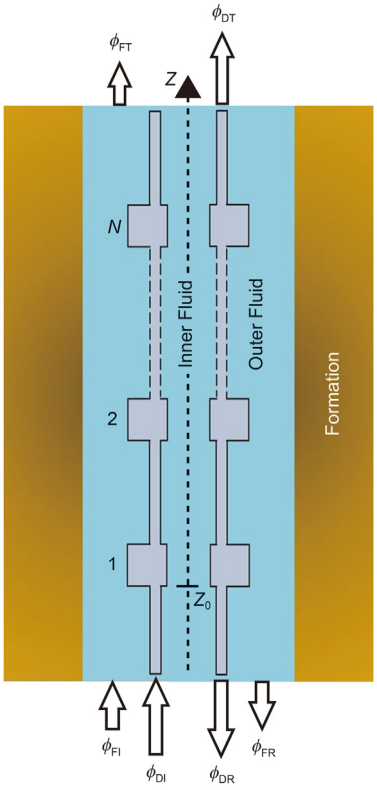

Fig. 4. The 1-D modeling of the DAT channel. The drill string contains N tool joints. Φ_{FI}, Φ_{FR}, and Φ_{FT} denote the amplitudes of the incident, reflected, and transmitted fluid waves, respectively; Φ_{DI}, Φ_{DR}, and Φ_{DT} denote the amplitudes of the incident, reflected, and transmitted drill-string waves, respectively.

propagating in the z-direction and can be represented by displacement potentials as

$$\varphi_f = \left(\Phi_f^+ e^{ik_f z} + \Phi_f^- e^{-ik_f z}\right)\cdot e^{i\omega t} \tag{6}$$

$$\varphi_d = \left(\Phi_d^+ e^{ik_d z} + \Phi_d^- e^{-ik_d z}\right)\cdot e^{i\omega t} \tag{7}$$

where Φ_f^+ and Φ_f^- denote the amplitudes of the fluid wave propagating in the positive and negative z-directions, respectively; Φ_d^+ and Φ_d^- denote the amplitudes of the drill-string wave propagating in those two opposite directions; k_f and k_d are the mode wavenumbers of the fluid wave and the drill-string wave solved by Eq. (1), both as functions of frequency; $e^{i\omega t}$ is the simple harmonic term of time and will be omitted in the subsequent derivation. By introducing the mode wavenumber, 1-D waves can also interact with the fluid-filled borehole.

When propagating along the z-axis, mode waves are reflected, transmitted, and converted at the interface connecting the tool joint and the drill pipe. We apply four continuity conditions to characterize these wave behaviors at the periodic interfaces. The continuous quantities are the fluid pressure p, the axial force of the drill string F, the axial displacement of the drill string u_d, and the relative volume velocity of the fluid V_f, respectively. Taking the interface $z = z_0$ in Fig. 4 as an example, we can get

$$p(z_0^-) = p(z_0^+) \tag{8}$$

$$F(z_0^-) = F(z_0^+) \tag{9}$$

$$u_d(z_0^-) = u_d(z_0^+) \tag{10}$$

$$V_f(z_0^-) = V_f(z_0^+) \tag{11}$$

where

$$p = \rho_f \omega^2 \varphi_f \tag{12}$$

$$F = -ES_d \frac{\partial u_d}{\partial z} \tag{13}$$

$$u_d = \frac{\partial \varphi_d}{\partial z} \tag{14}$$

$$V_f = S_f \frac{\partial\left(u_f - u_d\right)}{\partial t} \tag{15}$$

where z_0^- and z_0^+ indicate the lower and upper sides of the interface, respectively; E is Young's modulus of the drill string; $u_f = \partial\varphi_f/\partial z$ is the axial displacement of the fluid; S_d is the cross-section area of the drill string; in particular, if the fluid wave here is the outer Stoneley wave, S_f indicates the cross-section area of the outer fluid; else if the inner Stoneley wave, S_f indicates the cross-section area of the inner fluid. The relative volume velocity V_f in Eq. (15) is a physical expression representing the mode conversion of the drill-string wave to the fluid wave (Muggletona and Brennan, 2005). Then, Eqs. 8–11 can be written as a matrix equation

$$\mathbf{A_2}\cdot\mathbf{X}(z_0^-) = \mathbf{A_1}\cdot\mathbf{X}(z_0^+) \tag{16}$$

where

$$\mathbf{X} = \begin{bmatrix} \Phi_f^+ & \Phi_d^+ & \Phi_f^- & \Phi_d^- \end{bmatrix}^T \tag{17}$$

$$\mathbf{A}_j = \begin{bmatrix} \rho_f\omega^2 & 0 & \rho_f\omega^2 & 0 \\ 0 & ES_{dj}k_{dj}^2 & 0 & ES_{dj}k_{dj}^2 \\ 0 & ik_{dj} & 0 & -ik_{dj} \\ ik_{fj}S_{fj} & -ik_{dj}S_{fj} & -ik_{fj}S_{fj} & ik_{dj}S_{fj} \end{bmatrix}, (j = 1, 2) \tag{18}$$

where the subscript $j = 1$ denotes the tool joint section and $j = 2$ the drill pipe section. Let the length of the tool joint be L_1, and the length of the drill pipe be L_2, then the length of one periodic unit of the drill string is $L = L_1 + L_2$. Repeating the above continuity conditions, we can obtain the propagation equation for a periodic unit as

$$\mathbf{X}(z_0^-) = \left(\mathbf{A}_2^{-1}\cdot\mathbf{A}_1\cdot\mathbf{P}_1^{-1}\cdot\mathbf{A}_1^{-1}\cdot\mathbf{A}_2\cdot\mathbf{P}_2^{-1}\right)\cdot\mathbf{X}(z_0^- + L) \tag{19}$$

where

$$\mathbf{P}_j = \begin{bmatrix} e^{ik_f L_j} & 0 & 0 & 0 \\ 0 & e^{ik_d L_j} & 0 & 0 \\ 0 & 0 & e^{-ik_f L_j} & 0 \\ 0 & 0 & 0 & e^{-ik_d L_j} \end{bmatrix}, (j = 1, 2) \tag{20}$$

$\mathbf{P}_j$ represents the propagation of waves between two adjacent interfaces. According to the study of Lévesque and Piché (1992), the

formula written as Eq. (19) can greatly improve the numerical stability of the propagation matrix algorithm in the case of a large frequency-thickness product. Let $\mathbf{B} = (\mathbf{A}_2^{-1} \cdot \mathbf{A}_1 \cdot \mathbf{P}_1^{-1} \cdot \mathbf{A}_1^{-1} \cdot \mathbf{A}_2 \cdot \mathbf{P}_2^{-1})$. Then the propagation matrix is derived as $\mathbf{M}_N = \mathbf{P}_2^{-1} \cdot \mathbf{B}^N$ for the DAT channel containing N tool joints. Assuming that there are only transmitted waves but no reflected waves at the ground end of the channel, as shown in Fig. 4, the propagation equation can be obtained as

$$\begin{bmatrix} \Phi_{\mathrm{FI}} \\ \Phi_{\mathrm{DI}} \\ \Phi_{\mathrm{FR}} \\ \Phi_{\mathrm{DR}} \end{bmatrix} = \mathbf{M}_N \cdot \begin{bmatrix} \Phi_{\mathrm{FT}} \\ \Phi_{\mathrm{DT}} \\ 0 \\ 0 \end{bmatrix} \tag{21}$$

where Φ_{FI}, Φ_{FR}, and Φ_{FT} denote the amplitudes of the incident, reflected, and transmitted fluid waves, respectively; Φ_{DI}, Φ_{DR}, and Φ_{DT} denote the amplitudes of the incident, reflected, and transmitted drill-string waves, respectively. We rearrange the input and output ports of the DAT channel and rewrite Eq. (21) as

$$\begin{bmatrix} \Phi_{\mathrm{FR}} \\ \Phi_{\mathrm{DR}} \\ \Phi_{\mathrm{FT}} \\ \Phi_{\mathrm{DT}} \end{bmatrix} = \mathbf{W}_N \cdot \begin{bmatrix} \Phi_{\mathrm{FI}} \\ \Phi_{\mathrm{DI}} \\ 0 \\ 0 \end{bmatrix} \tag{22}$$

where the scattering matrix $\mathbf{W}_N$ is

$$\mathbf{W}_N = \begin{bmatrix} \mathbf{R}_{11} & \mathbf{T}_{N1} \\ \mathbf{T}_{1N} & \mathbf{R}_{NN} \end{bmatrix} \tag{23}$$

where the reflection coefficient matrix $\mathbf{R}_{11}$ represents the waves incident into periodic unit 1 and reflected; the reflection coefficient matrix $\mathbf{R}_{NN}$ represents the waves incident into periodic unit N and reflected; the transmission coefficient matrix $\mathbf{T}_{1N}$ represents the waves incident into periodic unit 1 and transmitted out from periodic unit N; the transmission coefficient matrix $\mathbf{T}_{N1}$ represents the waves incident into periodic unit N and transmitted out from periodic unit 1. Each matrix contains four coefficients, and the transmission coefficient matrix $\mathbf{T}_{1N}$ is what we need. The formula is as follows

$$\mathbf{T}_{1N} = \begin{bmatrix} t_{\mathrm{ff}} & t_{\mathrm{df}} \\ 0 & t_{\mathrm{dd}} \end{bmatrix} \tag{24}$$

Here, $t_{\mathrm{ff}} = \Phi_{\mathrm{FT}}/\Phi_{\mathrm{FI}}$ is the transmission coefficient of the fluid wave; $t_{\mathrm{dd}} = \Phi_{\mathrm{DT}}/\Phi_{\mathrm{DI}}$ is the transmission coefficient of the drill-string wave; $t_{\mathrm{df}} = \Phi_{\mathrm{FT}}/\Phi_{\mathrm{DI}}$ is the conversion coefficient of the drill-string wave. All three coefficients are functions of frequency. Putting the amplitudes of incident waves $\Phi_{\mathrm{FI}} = \mathrm{Exc_f}(\omega)/\rho_{\mathrm{f}}\omega^2$ and $\Phi_{\mathrm{DI}} = \mathrm{Exc_d}(\omega)/\rho_{\mathrm{f}}\omega^2$, where $\mathrm{Exc_f}(\omega)$ and $\mathrm{Exc_d}(\omega)$ are the excitation functions of the fluid wave and drill-string wave solved by Eq (5), respectively. The channel function of the DAT channel can be given as follows

$$H(\omega) = t_{\mathrm{ff}} \cdot \mathrm{Exc_f}(\omega) + \left(t_{\mathrm{df}} + t_{\mathrm{dd}}\right) \cdot \mathrm{Exc_d}(\omega) \tag{25}$$

Note that cases of the outer Stoneley wave and the inner Stoneley wave should be calculated separately and then taken into account in Eq. (25). The channel function $H(\omega)$ can be expressed as $H(\omega) = |H(\omega)| \cdot e^{i\theta(\omega)}$. $|H(\omega)|$ indicates the amplitude-frequency response of the channel, while the phase-frequency response $\theta(\omega)$ can be further derived as the group delay

$$G(\omega) = -\frac{\mathrm{d}}{\mathrm{d}\omega}[\theta(\omega)] \tag{26}$$

In addition, the full-wave impulse response of the channel can be calculated by the inverse Fourier transform as follows

$$h(t) = \frac{1}{2\pi}\int_{-\infty}^{+\infty} H(\omega) \cdot \mathrm{e}^{\mathrm{i}\omega t}\mathrm{d}\omega \tag{27}$$

The amplitude-frequency response, group delay, and impulse response will be used together to investigate the channel response.

3. Results and discussion

3.1. Algorithm correction and validation

To validate the effectiveness of the proposed method, we design a single-tool-joint model and compare the synthetic waveforms with the 2-D finite-difference time-domain (FDTD) method (Randall et al., 1991). Fig. 5a displays the single-tool-joint model with the source fixed on the outer surface of the drill pipe while the receiver is mounted on the inner surface of the drill pipe. The receiver-to-source axial distance is $z = 7.5$ m, and the tool joint length $L_1 = 0.5$ m. For the velocity–stress staggered grid 2-D FDTD in the cylindrical coordinates, the space steps are $\Delta r = 0.001$ m, $\Delta z = 0.01$ m, and the time step is $\Delta t = 1 \times 10^{-7}$ s. Perfect matching layers are applied around the FDTD model to eliminate artificial reflections, except on the borehole axis. Other model parameters are listed in Table 1. The dissipation effects of the fluid-filled borehole are ignored here to facilitate modeling. Fig. 5b presents the comparisons of waveforms simulated by the FDTD method, the proposed method, and the classic method (Wang et al., 2006). The source function is the cosine envelope pulse with a center frequency of 4 kHz, and its specific expression is given by He et al. (2013). For the proposed method, the synthetic waveform can be calculated as follows

$$s(t) = \frac{1}{2\pi}\int_{-\infty}^{+\infty} H(\omega)S(\omega) \cdot \mathrm{e}^{\mathrm{i}\omega t}\mathrm{d}\omega \tag{28}$$

where $S(\omega)$ is the spectrum of the source function; $H(\omega)$ is the channel function obtained from Eq. (25). In Fig. 5b, it can be distinguished three arrivals in the waveforms synthesized by the FDTD method, which are the transmitted drill-string wave, the converted fluid wave, and the transmitted fluid wave, respectively. The classic method only simulates the transmitted drill-string wave due to neglecting the coupling between the drill string and the fluid-filled borehole. In contrast, the proposed method can simulate the converted and transmitted fluid waves, but the amplitude of the converted fluid wave is underestimated. This underestimation is because we simplify the conversion process to the continuity of the relative volume velocity, as expressed by Eq. (15), and ignore the radial scattering of waves at the interface. Therefore, the channel function $H(\omega)$ in Eq. (25) needs to be corrected. By introducing a constant variable, namely the conversion intensity η_{c}, the channel function can be re-derived as

$$H(\omega) = t_{\mathrm{ff}} \cdot \mathrm{Exc_f}(\omega) + \left(\eta_{\mathrm{c}} \cdot t_{\mathrm{df}} + t_{\mathrm{dd}}\right) \cdot \mathrm{Exc_d}(\omega) \tag{29}$$

where t_{ff}, t_{df}, and t_{dd} can be calculated by Eq. (24). Substituting the new channel function $H(\omega)$ obtained from Eq. (29) into Eq. (28), we can get the corrected waveform. In Fig. 5b, the conversion intensity

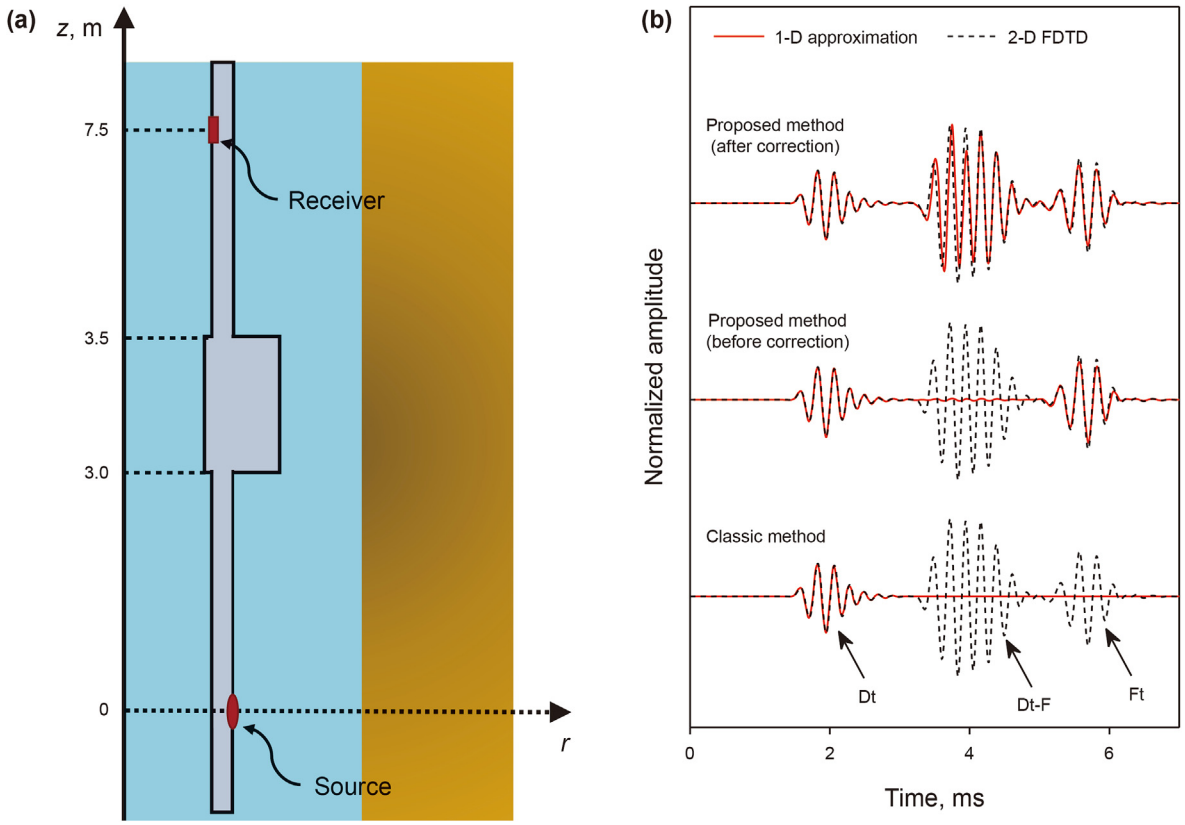

Fig. 5. Comparisons of synthetic waveforms for a single-tool-joint model. (a) The sketch of the 2-D modeling. The dissipation effects of the fluid-filled borehole are ignored to facilitate modeling, and the source function is the cosine envelope pulse with a center frequency of 4 kHz. (b) Comparisons of the synthetic waveforms are calculated by the 2-D finite-difference and 1-D approximation methods. The proposed method is corrected by a constant variable, namely conversion intensity η_c. The Dt, Dt-F, and Ft indicate the transmitted drill-string wave, the converted fluid wave, and the transmitted fluid wave, respectively.

is set as $\eta_c = 64$ according to the maximum value of the cross-correlation between two waveforms simulated by the proposed method and the FDTD method. After the correction, these two waveforms match very well, and the cross-correlation between them is 0.942. Thus, the accuracy of the proposed algorithm is well validated. It should be noted that the difference between these two methods would be smaller if smaller grids were used. We have tested it by refining the $\Delta z = 0.005$ m, but we do not present it here. The simulation results in Fig. 5b also illustrate that the mode conversion caused by the tool-joint scattering can be very significant.

Summarizing the above analyses, we give the following specific steps for correcting the channel modeling.

Step 1 Design a single-tool-joint channel model. The source transmits a pulse signal with a short duration, such as the cosine envelope pulse, in order to distinguish the arrival of several wave components at the receiver side. Calculate the received waveform based on the 2-D FDTD method and the 1-D modeling method, respectively, using the same model parameters.

Step 2 Determine the conversion intensity of the drill-string wave. The received waveforms obtained by the two methods are compared, and the conversion intensity is adjusted according to the cross-correlation value of the waveforms. The conversion intensity that maximizes the cross-correlation is determined as the correction value.

Step 3 Correct the channel function. The corrected conversion intensity is brought into Eq. (29). By characterizing the drill string as four-port propagation matrices, the channel response can be quickly obtained for any well depth.

The actual DAT channel contains numerous tool joints, and its axial length is much larger than its radial length. For such an excessively elongated model, the FDTD method fails to absorb artificial reflections from the radial boundaries of the computational domain in receiving long-time waveforms. By contrast, the proposed hybrid method calculates the channel response in the frequency domain with high accuracy and is more suitable for DAT channel modeling.

3.2. Simulations of transmitted and converted waves

In the following sections, the channel model for simulations consists of 9 tool joints and 10 drill pipes (i.e., $N = 9$). The tool joint length $L_1 = 0.5$ m, the drill pipe length $L_2 = 9.0$ m, and the total channel length is 94.5 m. Detailed parameters necessary for calculations are listed in Table 1. The quality factor of the formation in Table 1 is for both P and S waves.

Wave components in the DAT channel can be divided into transmitted and converted waves which need to be simulated and discussed separately. Fig. 6 presents the simulation results of the transmitted drill-string and fluid waves. According to Eq. (24), the amplitude-frequency responses are the absolute values of the coefficients t_{dd} and t_{ff}, while the corresponding time-domain results can then be calculated by the inverse Fourier transform. First, we analyze the amplitude-frequency response. Due to the periodic structure of the channel model, waves transmit with the comb-like characteristics of alternating pass-stop bands in the frequency domain, as shown in Fig. 6a, c, and 6e. If n denotes the number of the stopband, Drumheller and Knudsen (1995) have given an

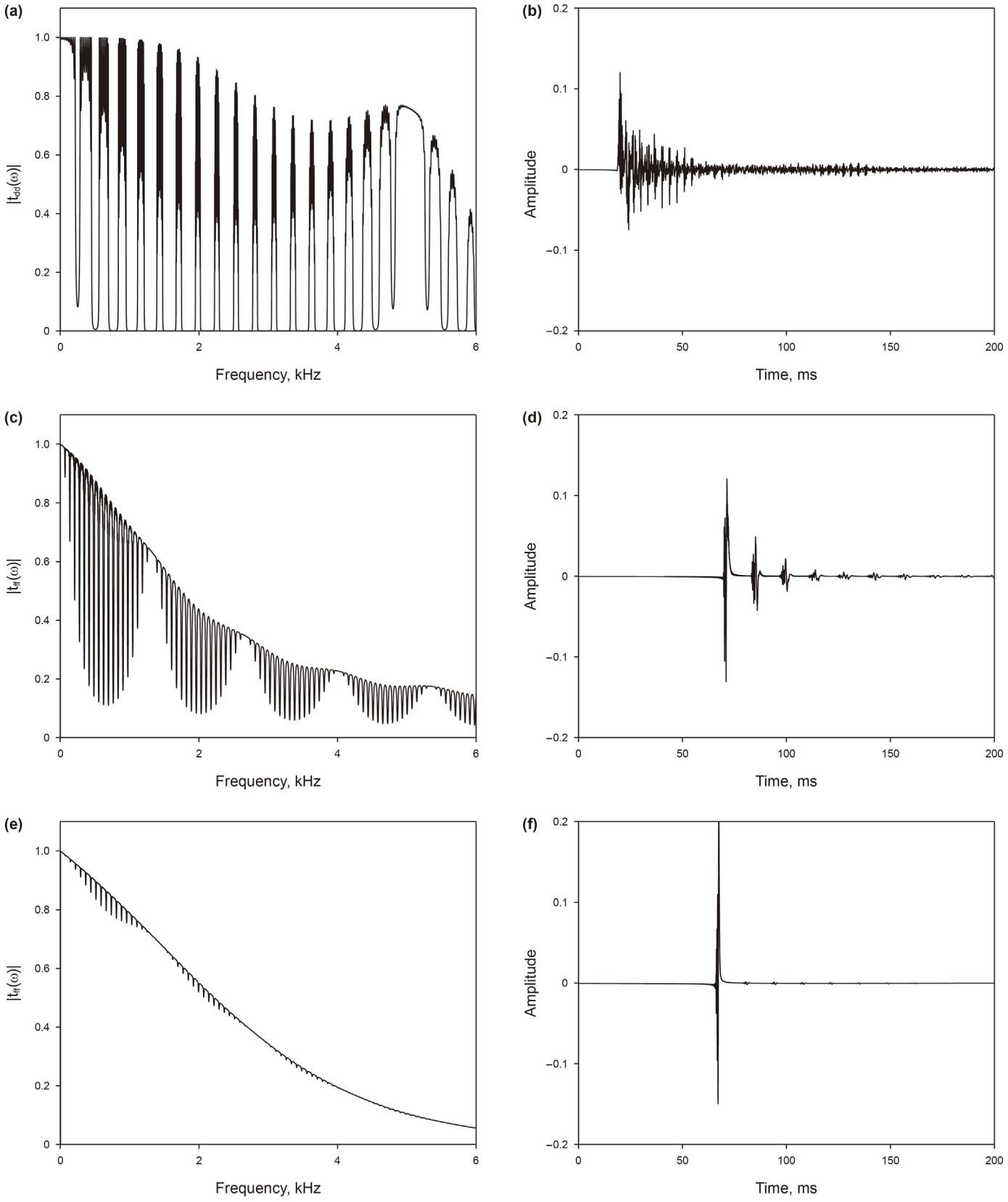

Fig. 6. The transmitted waves in the DAT channel. The amplitude-frequency and time-domain responses of the transmitted (a) (b) drill-string wave, (c) (d) outer Stoneley wave, and (e) (f) inner Stoneley wave. The channel model for simulations consists of 9 tool joints and 10 drill pipes, and the total length is 94.5 m.

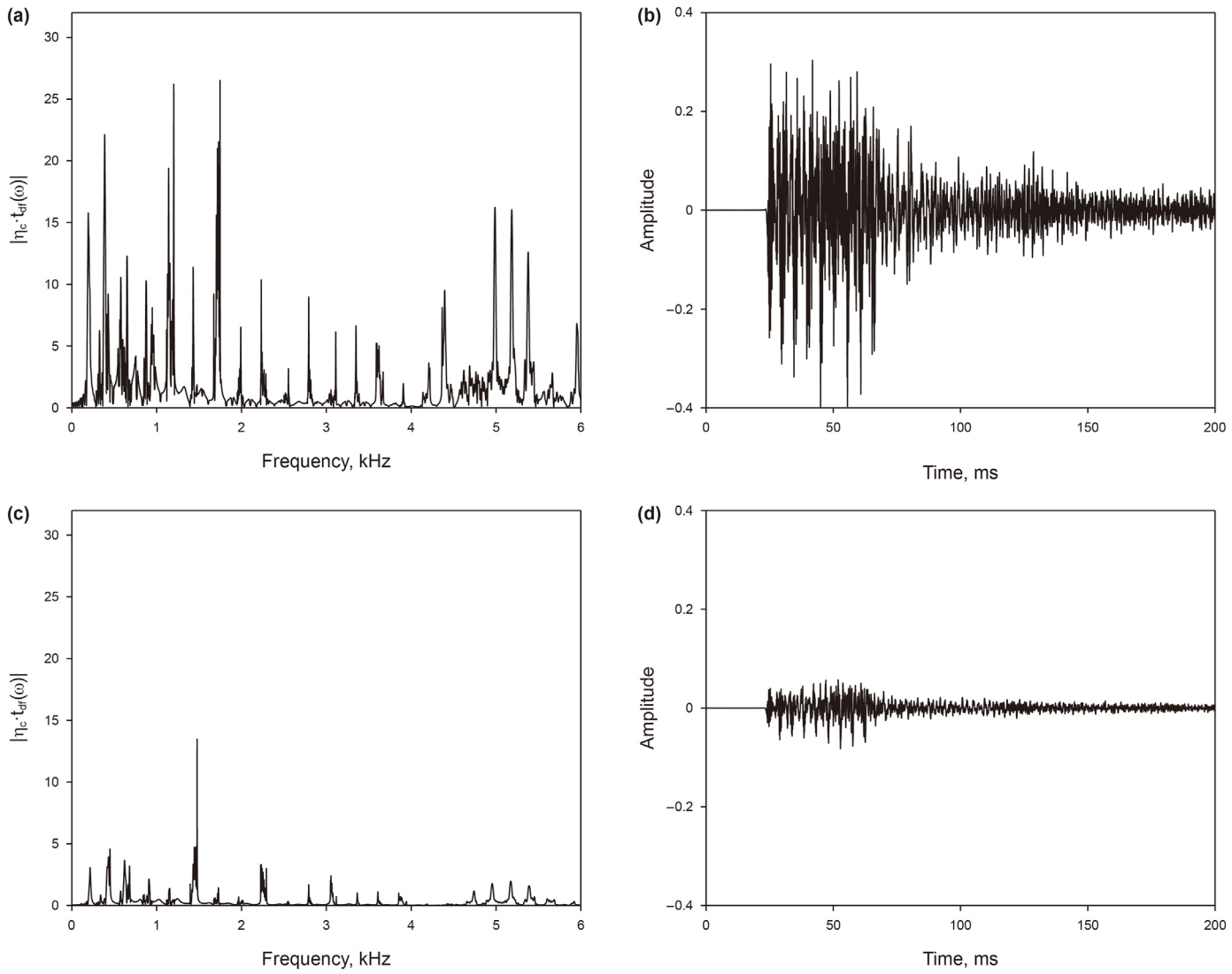

Fig. 7. The converted waves in the DAT channel, whose amplitudes are corrected by setting the conversion intensity $\eta_c = 64$. The amplitude-frequency and time-domain responses of the converted (a) (b) outer Stoneley wave, and (c) (d) inner Stoneley wave.

empirical formula for calculating the center frequency of the nth stopband

$$f_{\text{stop}} = n \cdot \frac{v_{\text{phase}}(0)}{2(L_1 + L_2)}, (n = 1, 2, 3, \ldots) \tag{30}$$

It can be read from Fig. 2a that the phase velocity of the drill-string wave at the zero frequency is 5071 m/s, so the nth stopband frequency is around 267n Hz according to the above relation. Similarly, the zero-frequency phase velocity of the outer Stoneley wave is 1318 m/s, so the nth stopband frequency is around 69n Hz. According to the phononic crystal theory, besides the alternating pass-stop bands, there are also half-wavelength passbands controlled by the tool joint length in the wave transmission. The center frequency of the mth half-wavelength passband can be evaluated as

$$f_{\text{half}} = m \cdot \frac{v_{\text{phase}}(0)}{2L_1}, (m = 1, 2, 3, \ldots) \tag{31}$$

According to Eq. (31), the mth half-wavelength passband of the drill-string wave is around $f_{\text{half}} = 5071\ m$ Hz, and the outer Stoneley wave corresponds to $f_{\text{half}} = 1318\ m$ Hz. In Fig. 6a and 6c, it can be observed that the drill-string wave contains one half-wavelength passband within 6 kHz, while the outer Stoneley wave contains four half-wavelength passbands. The amplitude-frequency characteristic of the inner Stoneley wave is roughly the same as that of the outer Stoneley wave. Fig. 6e illustrates that the bandgaps caused by the inner fluid are not significant compared with those in the outer fluid because of smaller changes in the cross-section area. As for the time-domain results shown in Fig. 6b, d, and 6f, it is found that all transmitted waves exhibit multiple arrivals caused by the reflections of periodic tool joints.

Fig. 7 presents the simulation results of the converted fluid waves, calculated by the coefficient t_{df} in Eq. (24). The amplitude-frequency response $\left|\eta_c \cdot t_{\text{df}}\right|$ is determined by setting conversion

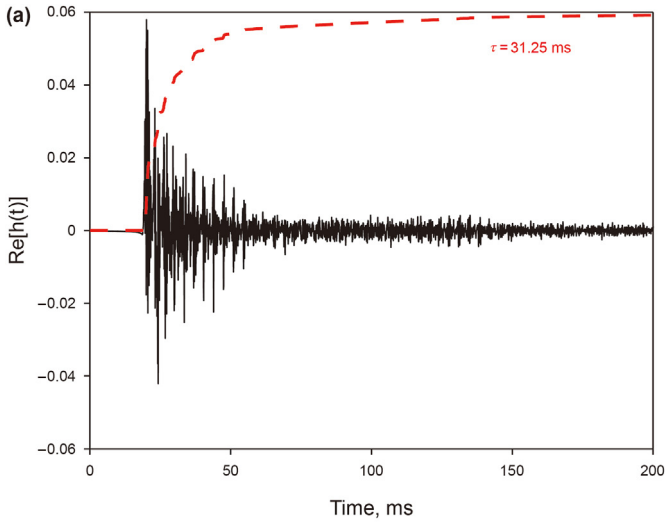

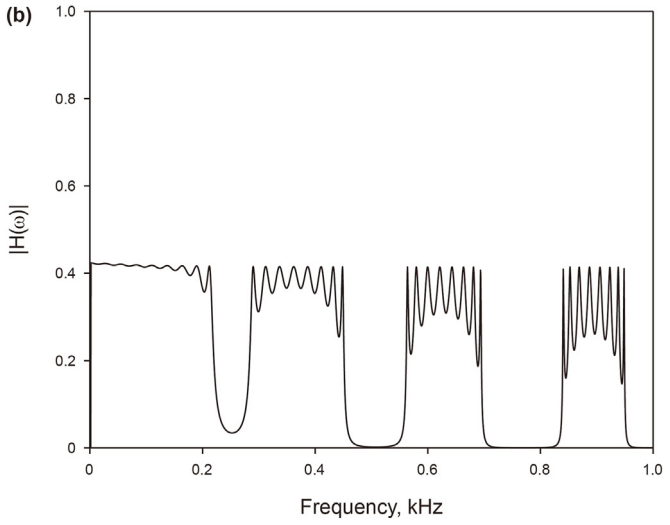

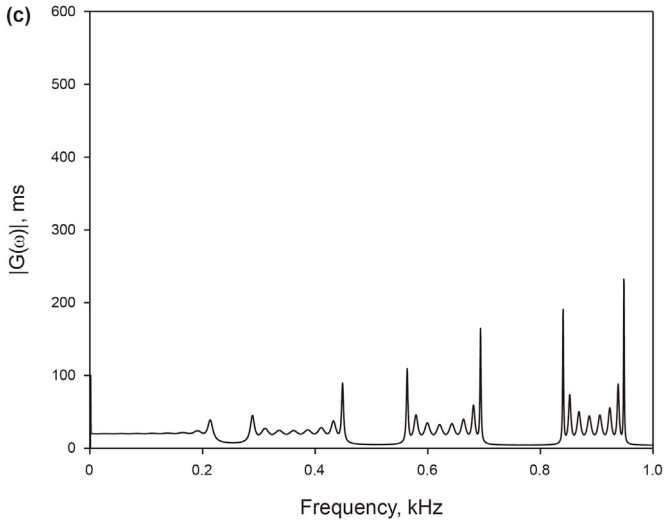

Fig. 8. The drill-string channel responses in a vacuum are evaluated by the (a) impulse response, (b) amplitude-frequency response, and (c) group delay. The delay spread of the channel is defined as the time duration required for the power of the impulse response to increasing to 90% of the total power. The red dashed line represents the power accumulation over time, and the delay spread τ is labeled.

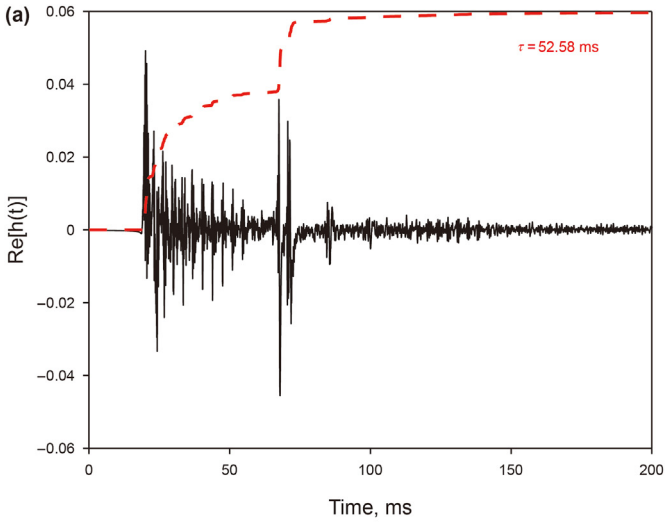

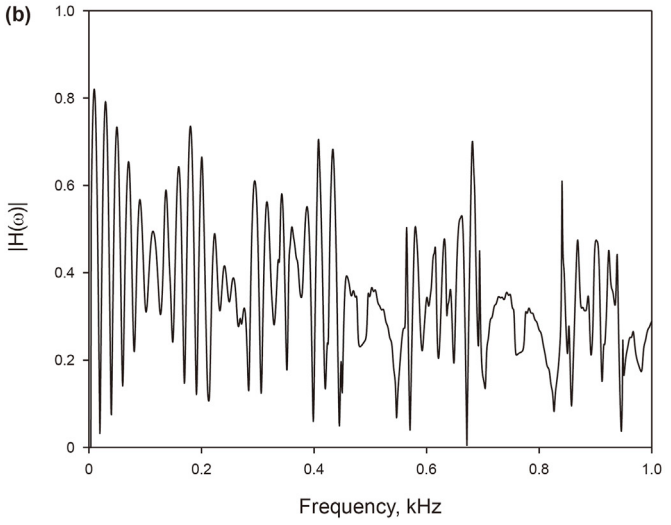

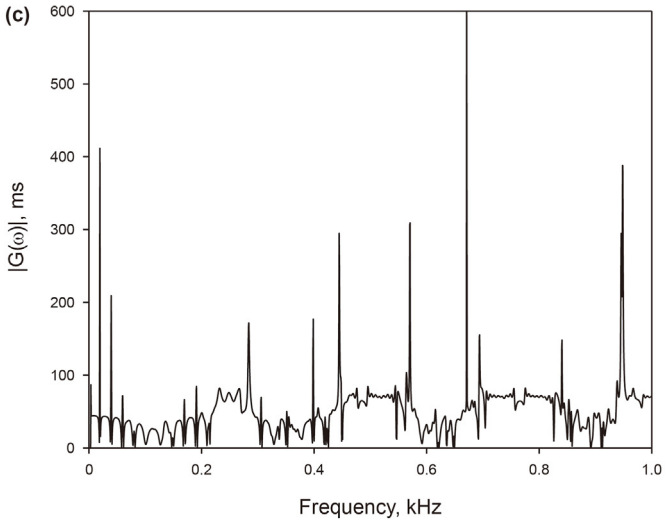

Fig. 9. The DAT channel responses are evaluated by the (a) full-wave impulse response, (b) amplitude-frequency response, and (c) group delay. The mode conversion is weak (i.e., $\eta_c = 1$) in this case, and the transmitted fluid waves are the primary interference to the channel.

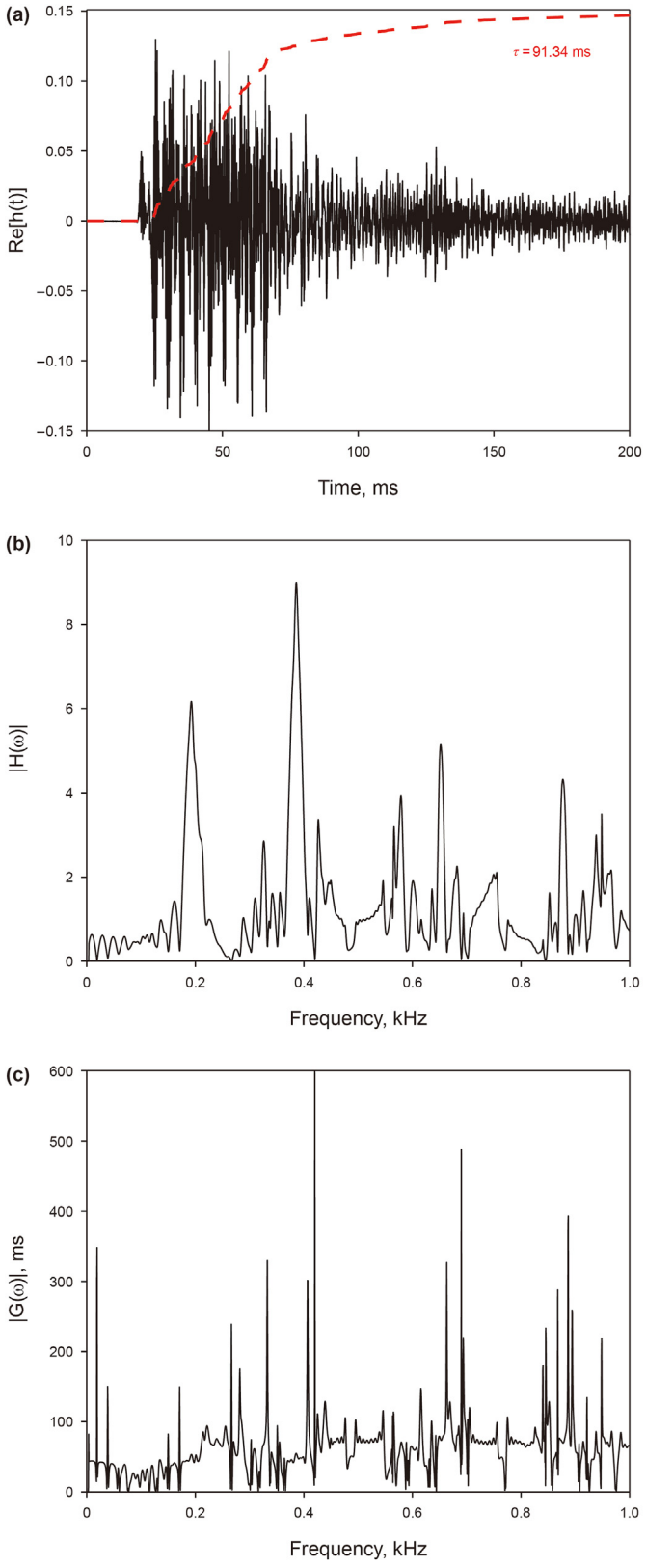

Fig. 10. The DAT channel responses are evaluated by the (a) full-wave impulse response, (b) amplitude-frequency response, and (c) group delay. The amplitudes of the converted fluid wave in the channel function are corrected by setting conversion intensity $\eta_c = 64$.

intensity $\eta_c = 64$, which is based on the comparison of synthetic waveforms in Fig. 5b. For the frequency-domain results shown in Fig. 7a and 7c, the sharp peaks of the converted fluid wave mainly appear at the positions of the drill-string-wave passbands (see Fig. 6a). The time-domain results in Fig. 7b and 7d shows that the converted fluid waves have strong amplitudes and long duration. Besides, the conversions that occur in the inner fluid are weaker than that in the outer fluid, which is still due to the difference in the variations of the cross-section area (Muggletona and Brennan, 2005). These observations are consistent with the physical understanding that the mode conversion occurs accompanied by the scattering of drill-string waves.

3.3. Comparative analyses of channel responses

Fig. 8 presents the responses of the drill-string channel in a vacuum. This case can simulate the ground or gas well situations and will be a reference for the DAT channel response. For the drill string in a vacuum, the channel response includes only the transmitted drill-string wave, with no propagation losses. The red dashed line plotted in Fig. 8a represents the power accumulation over time, and the delay spread τ is labeled. The delay spread of the channel is defined as the time duration required for the power of the impulse response to increasing to 90% of the total power. For the convenience of observation, only the first four passbands of the drill-string wave are displayed in Fig. 8b–c. It can be seen that the bandgap distribution of the drill-string channel is regular, and passbands appear periodically.

Figs. 9 and 10 present the DAT channel responses with different conversion intensities. According to Eq. (29), the channel function is formulated as a weighted sum of all wave components based on the excitation function. Then the group delay and full-wave impulse response can be obtained by substituting the channel function into Eqs. (26) and (27). The adjustment of the conversion intensity allows us to separately analyze the impact of the transmitted and converted fluid waves on the channel response. Fig. 9 presents the case with weak mode conversion (i.e., $\eta_c = 1$), in which the transmitted fluid waves are the primary interference to the channel. Fig. 9a shows that the delay spread of the DAT channel is increased by 68.25% compared to the vacuum case. As for the frequency responses, transmitted fluid waves lead to strong frequency selectivity within the passbands of the drill-string wave, as shown in Fig. 9b and c. Fig. 10 shows the case with strong mode conversion (i.e., $\eta_c = 64$). After considering the interference of the converted fluid waves, the delay spread of the DAT channel is further increased by 192.29% compared to the vacuum case, as shown in Fig. 10a. The amplitude-frequency response in Fig. 10b reveals that passband distributions in the DAT channel, distinguished from Fig. 8b, are rearranged. This theoretical result can explain the passband shifts in the field data (Drumheller, 1993; Drumheller and Knudsen, 1995) and also suggests that the drill-string response obtained from the ground test is unreliable. In addition, more troublesome, Fig. 10c demonstrates that the transmitted and converted fluid waves make the channel suffer from severe phase distortion, which is very detrimental to coherent demodulation.

3.4. Carrier modulation and data transmission

In wireless telemetry, baseband data is often sent out after modulating on a high-frequency carrier signal to use band resources fully. Therefore, observing the single-frequency carrier

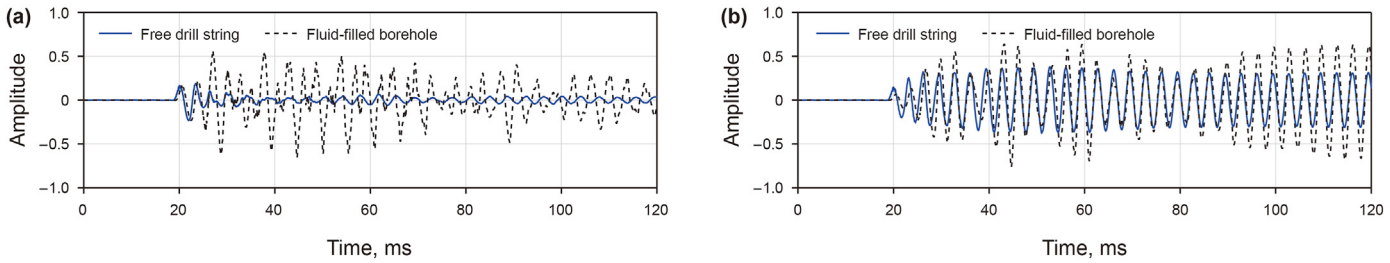

Fig. 11. Comparisons of carrier modulation in two channels at carrier frequencies (a) $f_c = 260$ Hz and (b) $f_c = 300$ Hz. DAT channel corresponds to the fluid-filled borehole environment with conversion intensity $\eta_c = 64$. The signal corresponding to the fluid-filled borehole in Fig. 11b is scaled by 0.5 when displayed.

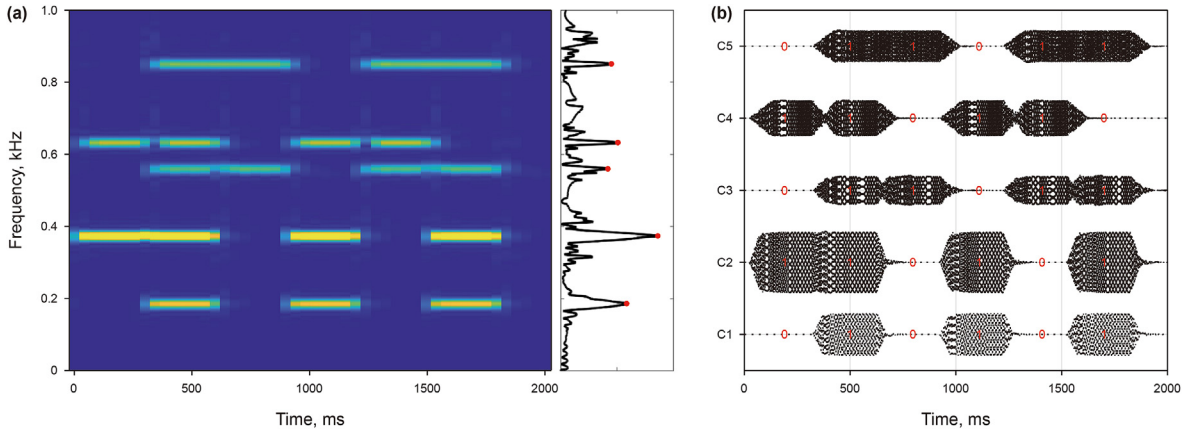

Fig. 12. The receiving and demodulation of the synthetic data on five carriers selected as the peak positions in the DAT channel response. (a) Time-frequency spectrum processing at the receiving side and the (b) received signals of each carrier are given. The symbol interval is set to 300 ms, and the transmission distance is 94.5 m. Data transmission is performed using OOK modulation and non-coherent demodulation.

modulations in the DAT channel is of practical significance. The carrier signal function is

$$c(t) = A_c \cos(2\pi f_c t) \tag{32}$$

where A_c is carrier amplitude; f_c is the center frequency. In Fig. 11, we design the carrier modulations for two center frequencies $f_c = 260$ Hz and $f_c = 300$ Hz, located at the stop and pass bands of the drill-string wave, respectively. DAT channel corresponds to the fluid-filled borehole environment with the conversion intensity set $\eta_c = 64$. The simulation results in the vacuum environment are still given as comparisons. With the interferences of fluid waves to the DAT channel, the amplitude and phase of the received signals show considerable distortions. Combined with the analyses in section 3.3, we can conclude that the DAT channel exhibits the characteristics of a multi-path coherent channel. Therefore, the conventional phase modulation and coherent demodulation may not apply to DAT. In addition, from Fig. 11a, carrier waves with considerable amplitudes pass through the DAT channel even if the drill-string wave is blocked. This observation further indicates that the drill-string passbands obtained by the ground test are unreliable.

Finally, we give an example of data transmission. Fig. 10b illustrates that the DAT channel still presents bandgap characteristics. Therefore, we select multiple carriers for data transmission simultaneously to fully utilize the bandwidth resources. We use on-off keying (OOK), a robust amplitude-modulation strategy, on each carrier to counteract the phase and amplitude distortions. Identification and demodulation of the data can be performed at the receiver side, combining a Fourier transform and envelope detection. As a non-coherent method, this demodulation strategy does not depend on the coherence of carriers. Fig. 12 presents the receiving and demodulation of the synthetic data on five carriers whose center frequencies are selected as the peak positions in the channel response. The time-frequency spectrum in Fig. 12a is obtained by the short-time Fourier transform. The black line represents the amplitude-frequency response of the channel within 1 kHz, and the red points mark the positions of five amplitude peaks. The frequencies corresponding to the amplitude peaks are used for carrier transmission. The transmission distance is 94.5 m with the conversion intensity set $\eta_c = 64$. The symbol interval is set to 300 ms, more than three times the delay spread. The demodulation results of the five carriers are labeled in Fig. 12b. Based on synthetic data, the communication scheme in Fig. 12 achieves a transmission rate of 15 bps in a 94.5 m long channel, which is higher than typical for commercial mud-pulse telemetry. Thus, in combination with carrier multiplexing and non-coherent demodulation, using the DAT channel for efficient data transmission is feasible. And for scenarios requiring higher transmission rates, spatial multiplexing and space-time coding techniques effectively counteract multi-path effects and can further improve the communication efficiency and reliability of the DAT channel.

4. Conclusions

This paper proposes a hybrid method to characterize the downhole-acoustic-telemetry (DAT) channel modeled in the logging-while-drilling (LWD) scenario. It is revealed that the wave components in the DAT channel can be distinguished as the drill-string wave, the transmitted fluid wave, and the converted fluid wave, and the channel function can be formulated as a weighted sum of these wave components. The transmitted and converted

waves together constitute the carrier wave, which is the essential feature of the DAT channel. Through the comparisons of synthetic waveforms for the case of a single-tool-joint model, we find our proposed method could provide consistent results with those of the 2-D finite-difference method at the frequency range for telemetry.

The transmitted and converted fluid waves interfere with the drill-string wave and result in considerable channel delays. As for the frequency responses, the DAT channel has the bandgap characteristic, but its passband distributions differ from the free drill string case. In addition, the phase-frequency response of the channel exhibits strong frequency selectivity. Therefore, the DAT channel can be considered a particular coherent multi-path channel. When evaluating channel capacity, the influence of the fluid-filled borehole environment cannot be ignored.

The carrier modulations illustrate that unpredictable amplitude and phase distortions may fail coherent demodulation. To address this channel characteristic, we give a robust strategy for data transmission that combines carrier multiplexing and non-coherent demodulation. By using synthetic data, the transmission rate can reach more than 15 bps in a 94.5 m long channel, which is higher than typical for commercial mud-pulse telemetry. The technical scheme of acoustic telemetry is expected to break the low-speed limitation of LWD data transmission.

Declaration of competing interest

The authors declare that they have no known competing financial interests or personal relationships that could have appeared to influence the work reported in this paper.

Acknowledgments

We are grateful for constructive comments from reviewers and the editor, which improve the quality of the paper. This study is supported by the National Natural Science Foundation of China (Grant Nos. 12174421 and 11734017) and the Scientific Instrument Developing Project of the Chinese Academy of Sciences, China (Grant Nos. YJKYYQ20200072 and GJJSTD20210008).

References

Carcione, J.M., Poletto, F., 2000. Simulation of stress waves in attenuating drill strings, including piezoelectric sources and sensors. J. Acoust. Soc. Am. 108 (1), 53–64. https://doi.org/10.1121/1.429443.

Cui, Z.W., 2004. Theoretical and Numerical Study of Modified Biot's Models, Acoustoelectric Well Logging and Acoustic Logging while Drilling Excited by Multipole Acoustic Sources (Ph.D. dissertation). Jilin University.

Drumheller, D.S., 1989. Acoustical properties of drill strings. J. Acoust. Soc. Am. 85 (3), 1048–1064. https://doi.org/10.1121/1.397488.

Drumheller, D.S., 1993. Attenuation of sound waves in drill strings. J. Acoust. Soc. Am. 94 (4), 2387–2396. https://doi.org/10.1121/1.407458.

Drumheller, D.S., Knudsen, S.D., 1995. The propagation of sound waves in drill strings. J. Acoust. Soc. Am. 97 (4), 2116–2125. https://doi.org/10.1121/1.412004.

Gao, L., Finley, D., Gardner, W., Robbins, C., Linyaev, E., Moore, J., Mmarzadeh, M., Johnson, D., 2006. Acoustic telemetry delivers more real-time downhole data in underbalanced drilling operations. In: Proceedings of IADC/SPE Drilling Conference. https://doi.org/10.2118/98948-MS.

Gutierrez-Estevez, M.A., Krueger, U., Krueger, K.A., Manolakis, K., Jungnickel, V., Jaksch, K., Krueger, K., Mikulla, S., Giese, R., Sohmer, M., Reich, M., 2013. Acoustic broadband communications over deep drill strings using adaptive OFDM. In: Proceedings of IEEE Wireless Communications and Networking Conference. https://doi.org/10.1109/WCNC.2013.6555232.

He, X., Hu, H.S., Wang, X.M., 2013. Finite difference modelling of dipole acoustic logs in a poroelastic formation with anisotropic permeability. Geophys. J. Int. 192 (1), 359–374. https://doi.org/10.1093/gji/ggs024.

He, X., Wang, X.M., Chen, H., 2017. Theoretical simulations of wave field variation excited by a monopole within collar for acoustic logging while drilling. Wave Motion 72, 287–302. https://doi.org/10.1016/j.wavemoti.2017.04.005.

Klotz, C., Bond, P., Wassermann, I., Priegnitz, S., 2008. A new mud pulse telemetry system for enhanced MWD/LWD applications. In: Proceedings of IADC/SPE Drilling Conference. https://doi.org/10.2118/112683-MS.

Kumar, L.S., Han, W.K., Guan, Y.L., Sun, S., Lee, Y.H., 2014. Optimal energy transfer pipe arrangement for acoustic drill string telemetry. IEEE Trans. Geosci. Rem. Sens. 52 (11), 6999–7007. https://doi.org/10.1109/TGRS.2014.2306686.

Kurkjian, A.L., 1985. Numerical computation of individual far-field arrivals excited by an acoustic source in a borehole. Geophysics 50 (5), 852–866. https://doi.org/10.1190/1.1441961.

Kurkjian, A.L., Chang, S.K., 1986. Acoustic multipole sources in fluid-filled boreholes. Geophysics 51 (1), 148–163. https://doi.org/10.1190/1.1442028.

Lee, H.Y., 1991. Drillstring Axial Vibration and Wave Propagation in Boreholes (Ph.D. dissertation). Massachusetts Institute of Technology.

Lévesque, D., Piché, L., 1992. A robust transfer matrix formulation for the ultrasonic response of multi-layered absorbing media. J. Acoust. Soc. Am. 92 (1), 452–467. https://doi.org/10.1121/1.404256.

Lous, N.J.C., Rienstra, S.W., Adan, I.J.B.F., 1998. Sound transmission through a periodic cascade with application to drill pipes. J. Acoust. Soc. Am. 103 (5), 2302–2311. https://doi.org/10.1121/1.422749.

Matuszyk, P.J., Torres-Verdín, C., 2014. Frequency-domain simulation of logging-while-drilling borehole sonic waveforms. Geophysics 79 (2), D99–D113. https://doi.org/10.1190/geo2013-0279.1.

Muggletona, J.M., Brennan, M.J., 2005. Axisymmetric wave propagation in buried, fluid-filled pipes: effects of wall discontinuities. J. Sound Vib. 281 (3–5), 849–867. https://doi.org/10.1016/j.jsv.2004.02.045.

Neff, J.M., Camwell, P.L., 2007. Field-test results of an acoustic MWD system. In: Proceedings of SPE/IADC Drilling Conference. https://doi.org/10.2118/105021-ms.

Pardo, D., Matuszyk, P.J., Torres-Verdin, C., Mora, A., Muga, I., Calo, V.M., 2013. Influence of borehole-eccentred tools on wireline and logging-while-drilling sonic logging measurements. Geophys. Prospect. 61 (1), 268–283. https://doi.org/10.1111/1365-2478.12022.

Rama Rao, V.N., Vandiver, J.K., 1999. Acoustics of fluid-filled boreholes with pipe: guided propagation and radiation. J. Acoust. Soc. Am. 105 (6), 3057–3066. https://doi.org/10.1121/1.424635.

Randall, C.J., Scheibner, D.J., Wu, P.T., 1991. Multipole borehole acoustic waveforms: synthetic logs with beds and borehole washouts. Geophysics 56 (11), 1757–1769. https://doi.org/10.1190/1.1442988.

Reeves, M.E., Camwell, P.L., Mcrory, J., 2011. High speed acoustic telemetry network enables real-time along string measurements, greatly reducing drilling risk. In: Proceedings of SPE Offshore Europe Oil and Gas Conference and Exhibition. https://doi.org/10.2118/145566-MS.

Shah, V., Gardner, W., Johnson, D.H., Sinanovic, S., 2004. Design considerations for a new high data rate LWD acoustic telemetry system. In: Proceedings of SPE Asia Pacific Oil and Gas Conference and Exhibition. https://doi.org/10.2118/88636-MS.

Sinha, B.K., Simsek, E., Asvadurov, S., 2009. Influence of a pipe tool on borehole modes. Geophysics 74 (3), E111–E123. https://doi.org/10.1190/1.3085644.

Tochikawa, T., Sakai, T., Taniguchi, R., Shimada, T., 1996. Acoustic telemetry: the new MWD system. In: Proceedings of SPE Annual Technical Conference and Exhibition. https://doi.org/10.2118/36433-MS.

Wang, C.Y., Qiao, W.X., Zhang, W.Q., 2006. Using transfer matrix method to study the acoustic property of drill strings. In: Proceedings of IEEE International Symposium on Signal Processing and Information Technology. https://doi.org/10.1109/ISSPIT.2006.270837.

Wassermann, I., Kaniappan, A., 2009. How high-speed telemetry affects the drilling process. J. Petrol. Technol. 61 (6), 26–29. https://doi.org/10.2118/0609-0026-JPT.

Yang, Y.F., Guan, W., Hu, H.S., Xu, M.Q., 2017. Numerical study of the collar wave characteristics and the effects of grooves in acoustic logging while drilling. Geophys. J. Int. 209 (2), 749–761. https://doi.org/10.1093/gji/ggx044.

Zheng, Y., Huang, X., Toksoz, M.N., 2004. A finite element analysis of the effects of tool eccentricity on wave dispersion properties in borehole acoustic logging while drilling. In: Proceedings of SEG Int'l Exposition and 74th Annual Meeting. https://doi.org/10.1190/1.1839721.

Zheng, L.C., Yu, J.Q., Yang, Q.H., Gao, Y., Sun, F.C., 2017. Vibration wave downhole communication technique. Petrol. Explor. Dev. 44 (2), 321–327. https://doi.org/10.1016/S1876-3804(17)30037-X.

Zheng, X.B., Hu, H.S., 2017. A theoretical investigation of acoustic monopole logging-while-drilling individual waves with emphasis on the collar wave and its dependence on formation. Geophysics 82 (1), D1–D11. https://doi.org/10.1190/geo2016-0266.1.